COO-088-36

A PRELIMINARY LOOK AT HADRON STRUCTURE WITH A DOUBLE ARM CALORIMETER*

Fermilab, Lehigh, Pennsylvania, Wisconsin

*Invited talk presented by A.E. Erwin at the Vanderbilt Conference March 6-8, 1978

A Preliminary Look at Hadron Structure With a Double Arm Calorimeter

Fermilab, Lehigh, Pennsylvania, Wisconsin Collaboration

This experiment is a collaborative effort by four institutions involving people shown in figure 1.

Figure 2 is an approximate plan view of the apparatus. The steel was part of a 24 absorption length hadron shield which effectively prevented small angle scatters upstream from simulating large P_T target events. A hydrogen target consisted of separate 12" and 6" segments for studying large P_T accidentals due to multiple interactions. Two of the six drift chamber planes achieved unique x-y readout on individual hits using cathode delay lines in addition to electron drift time.

Both calorimeter arms rested on a steel plate which moved along the beam line on rails. The right arm could be moved independently by jacking it along on a teflon pad. The right arm was a delux model calorimeter with an initial layer of Pb (5 radiation lengths) for π° identification followed by several layers of steel (each $\sim$ 2 absorption lengths) to observe hadron shower development. For financial reasons the left arm has smaller solid angle for hadrons and coarser spatial resolution. The left π° detector is quite efficient, however, with a thickness of 21 radiation lengths of Pb. A beam's-eye view of the calorimeters appears in figure 3.

Every one of the $\sim$ 150 elements in the calorimeters had an individual pulse height read-out and an unambiguous spatial coordinate. Unlike calorimeters with long scintillator slats, our calorimeters permitted a true P_T trigger to be formed by attenuating each pulse height an amount proportional to sin θ and adding the results. Typical running positions gave the left arm about 1 sr in the c.m.s. and the right arm about 1.5 sr. Azimuthal acceptances were $\sim \pm 40°$.

Figure 4 shows a simple scatter plot of vertex positions for a target empty run using the 2 largest angle tracks in the drift chambers. One sees these events originate mostly in the superinsulation and the beam counters. Events upstream of the target area would have presented serious difficulty.

Figure 5 shows the target empty data to be of the same character in P_T as the target full data. Up to 5 or 6 GeV/c in P_T it would not even appear important to make an empty subtraction. Target empty subtractions were nevertheless made.

There were three basic types of triggers used for physics analysis which we will now discuss. (L) or (R) triggers recorded data if the total P_T of one arm exceeded a preset threshold. Figure 6 shows a preliminary invariant cross section for jets at 400 GeV using an (R) trigger at two different thresholds. There is a rapid rise in cross section at threshold followed by the typical exponential fall off found in high P_T experiments using single particle triggers.

Figure 7 shows an effect that has been discussed[1] for single arm triggers but never so clearly seen in data as here. In the top histogram (right-side-up) we see a selected bin of P_T for events which produced a left arm (L) trigger. These events produce a spectrum of P_T in the right arm (inverted histogram) which peaks somewhat lower in P_T than the trigger arm. When the trigger P_T is increased in the left arm, we see in the second half of figure 7 that the peak in the right arm also increases but is still smaller than the trigger P_T.

This near-balance of P_T is summarized for several trigger values in figure 8. The fact that the away side has a systematically lower P_T might be explained in the context of a parton model by noting that transverse Fermi momentum of the partons would naturally conspire to deposit more momentum on the trigger side because of the steepness of the P_T spectrum.

In contrast to real events figure 8 also contains 3 points generated by a peripheral phase space program[2] for a 15 body final state. Lower multiplicities than 10 tend to give no high P_T single arm triggers. We see that even though an occasional phase space event gives a right arm trigger, the amount of P_T captured by the other arm is independent of the trigger P_T. Figure 9 shows peripheral phase space spectra for 20 body final states when the right side threshold is 1.5 GeV/c. Only 6.5% of these events make a right arm trigger, and only 25% of those give any P_T into the left arm.

(SPR) and (SPL) triggers were attempts to observe a single particle which carried unusually large p_T into the right trigger. A group of several contiguous segments was used for this trigger. Figure 10 shows the angular distribution of P_T about the centroid for such triggers. The P_T is indeed tightly collimated as one would expect for a single particle and is dramatically different from jet distributions.

An invariant cross section using single π° triggers (SPL) in the left arm is shown in figure 11. It agrees quite well with more precise π° data of others and thus gives us confidence in the energy calibration and interpretations of the single particle trigger.

The third trigger type (L + R) required the sum of the P_T magnitudes in the left and right calorimeter to exceed a preset value. Such a trigger would have no bias toward one arm or the other insofar as Fermi momentum of partons is concerned.

Figure 12 is a scatter plot of raw data taken with such a trigger at 400 GeV using a logarithmic intensity scale. Note the sharp threshold and the tendency for transverse momentum to balance in the two arms.

If we take a slice of data perpendicular to the 45° diagonal, we see in figure 13 the real extent of the P_T balance. The trigger itself does not a priori favor such a balance. To see this we can make a Monte Carlo model using what we do know from single particle high P_T data[3].

$$\text{i.e.} \quad \sigma_I\,(P_T) \sim P_T^{-8}(1-x_T)^9 \quad \text{where } x_T = 2\,P_T/\sqrt{s}$$

Our model will assume each arm obeys this distribution independently.

$$\sigma \sim \sigma_I(P_{TR}) \cdot \sigma_I(P_{TL})$$ where P_{TR} (P_{TL}) is P_T in the right (left) arm.

The result is shown as a dashed histogram in figure 13. Computational reasons prevent us from extending the Monte Carlo as far from the diagonal as the data, but the model clearly favors unbalanced P_T. Thus there appears to be a physics related correlation between the P_T collected in the two arms.

The peripheral phase space events mentioned earlier are highly discriminated against by the (L + R) trigger. These events drop off as $e^{-8.6P_T}$ and $e^{-7.6P_T}$ respectively for 15 and 20 body final states compared to real data which drop off like e^{-3P_T}.

Feynman and Field have suggested that the P_T bias of a single arm trigger for high P_T events might take a spectrum which would otherwise fall as P_T^{-6} and change it to a spectrum which falls as P_T^{-8}, a change of approximately 2 in the power of P_T. Since our (L + R) trigger does not exhibit this bias we have made a preliminary effort to look into this difficult and somewhat controversial matter.

We make the assumption that our invariant, double arm cross section obeys the form suggested by dimensional counting.

$$\sigma_I = \frac{d\sigma}{\frac{d^3p_1}{E_1}\frac{d^3p_2}{E_2}} = \frac{1}{P_T^{\,n}} f(x_T, \theta_{cms}) \text{ where } x_T = 2P_T/\sqrt{s}.$$

If scaling holds, one expects the power of n to be 6 for a double arm cross section instead of the usual n = 4 expected for a single arm cross section.[4] By comparing this cross section at two energies (200 GeV and 400 GeV) for the same x_T and θ_{cms} we can extract the power <u>n</u> without having to know the form of $f(x_T, \theta_{cms})$.

We make an effort to use the same detector solid angles $d\Omega_{Left}$ and $d\Omega_{Right}$ at 200 and 400 GeV/c so that we can use $\sigma_I \sim \frac{1}{P_T^{\,2}} \frac{d\sigma}{dP_T}$ for the cross section ratio of our double arm triggers at the two energies. The "P_T" assigned to an invididual event is taken to be the same for all events in a slice such as the one shown in figure 12. The P_T value is taken to be that of one arm when the P_T balance is perfect. Figure 14 is a plot proportional to $d\sigma/dP_T$ for data at 200 and 400 GeV in a limited range of P_T. Since $\sqrt{s}_{400}/\sqrt{s}_{200} = 1.41$, the two curves have approximately the same slope when plotted versus x_T.

The power of n that fits the data of figure 14 best at the highest P_T is $n = 7.8$. The power is two units higher than we expect from scaling but not the usual four units higher that one finds from single arm data. Using jets to obtain this power has some special difficulties, however, that need better understanding. The worst problem is that one does not know how to relate the amount of energy measured for the jet to the energy that it actually had except through the use of jet models.

Some of the problems one has with jets can be appreciated it one looks at a particular model for a jet. We will show one here which agrees with our data remarkably well so far. It is a suggestion by Selove based on an observation by Feynman that since $dN/dy \approx 2$ for ordinary backward/forward jets, it might also be true for high P_T jets. This leads to the conclusion (see figure 15) that the longitudinal momenta in an average jet drop off by factors of ~ 2.

In figure 16 is a plot of the distribution of momenta observed in whatever segment of the right arm calorimeter which happens to have the largest P_T. It is supposed that this momentum is directly related to that of the particle in the jet with the highest longitudinal momentum. Also shown is the distribution of momenta for whatever segment has the second highest P_T. We see that on the average these two momenta are in the ratio 2:1 as the model suggested.

Converted to a suitable Monte Carlo program, this model can predict the particle multiplicity that should be captured by one of our calorimeter arms. This prediction is shown in figure 17 as a function of jet P_T. An algorithm based on the number of calorimeter segments with energy above some minimum value can also give a measure of observed particle multiplicity. Because of finite shower size and sharing of some showers by adjacent segments, this algorithm probably over estimates the particle count by $\sim 2X$. The result seems to agree rather well with the jet model.

If what we see is not a jet but is instead a soft spray of average P_T particles, Sivers, Brodsky, and Blankenbecler[5] suggest that multiplicity should depend on P_T as $\langle n \rangle \approx P_T/\langle P_T \rangle$. The multiplicity algorithm does not agree with this at all as can be seen in figure 18.

By treating the individual particles in a jet as massless, one can obtain a mass spectrum for that part of a jet observed in a particular arm. Figure 19 is the mass spectrum for jets with $3.5 < P_T < 4.0$ GeV/c in the right arm which had a jet axis directed near the center of the arm. The average jet mass is about $2 GeV/c^2$. A width of $1 GeV/c^2$ indicates the calorimeter mass resolution is at least that good. Once again the Monte Carlo jet model agrees well with this spectrum.

Because the Monte Carlo jet model agrees so well in cases where it can be checked, we are inclined to believe its predictions for matters which are less directly observed. For instance, the calorimeter on the average misses a fixed amount of P_T ($\sim$1 GeV/c) regardless of the size of the P_T. Among other things this results in better angular definition of jet direction as P_T increases. Figure 20 shows the average difference expected between a measured jet direction and the true direction that would have been measured if all particles could have been collected by the calorimeter. Clearly, one cannot expect to obtain a sharp angular distribution in the c.m.s. for jets with P_T = 2GeV/c, however jets with P_T = 6 GeV/c can be defined to 5 degrees.

One of the original objectives of this experiment was to measure the difference between the pion and proton structure functions by studying the angular distribtuions of jets in the overall center of mass for the colliding hadrons. Figure 21 shows a naive picture for what one expects on the average. Partons in pions are thought to carry a larger fraction x of the hadron momentum than partons in a proton. Thus one should find <u>both</u> jets from the fragmenting partons in the forward hemisphere more frequently in πp collisions than in pp collisions.

In order to achieve independence of possible experimental difficulties what we plot in figure 22 is the ratio $R_{JET} = \sigma(pp \rightarrow Jets)/\sigma(\pi p \rightarrow Jets)$. The beam for this plot consisted of positive particles at 130 GeV/c, Cerenkov tagged. Jets with P_T between 2.5 and 2.75 GeV/c were used to determine cms angles. Results are qualitatively very much as one expects they would be if jets are the result of parton scattering.

1. E. Malmud, Proceedings of VIII International Symposium on Multiparticle Dynamics, Kayserberg, (1977).
2. A. E. Brenner, D. C. Carey, R. Pordes, and J. H. Friedman. NVERTX, A Computer Program for Monte Carlo Phase Space with Importance Sampling and Histogram Display. Fermilab preprint. We are indebted to D. Carey for his help with this program.
3. D. Antreasyan et al., Phys. Rev. Letters 38, 112 (1977).
4. We are indebted to Francis Halzen for discussions on this matter.
5. D. Sivers, Brodsky, R. Blankenbecler, Phys. Reports C23, (1976).

Figure Captions

Fig. 2 Schematic floor plan of the experimental apparatus.

Fig. 3 The two calorimeter arms as seen from the target.

Fig. 4 Target empty run. A plot of "interaction" vertices obtained by using the two largest angle tracks in each event. Clusters of vertices occur at the superinsulation for the two targets and at scintillation counters just before the target.

Fig. 5 Number of events versus P_T at 400 GeV for double arm (L + R) triggers. Target empty data has the same slope as target full data and accumulates at about 1/5 the rate of target full data.

Fig. 6 Preliminary estimate of the invariant cross section for 400 GeV pp events producing a jet using right arm (R) triggers.

Fig. 7 P_T spectrum for the calorimeter on the away side (inverted histogram) when the calorimeter on the trigger side has P_T in the bins shown (erect histogram).

Fig. 8 Relation between peak P_T on the away side to trigger P_T (solid curve). Three points generated by a 15 body phase space program illustrate the small extent to which P_T conservation forces particles into the away side at these values of x_T.

Fig. 9 Response of the calorimeters to 20 body events generated by invariant phase space times $\exp(-6P_T)$ when the right arm (R) threshold is set at P_T = 1.5 GeV/c.

Fig. 10 Distribution of P_T per unit solid angle away from the jet axis when a single particle (SPR) trigger is used. A random distribution of 2 or more particles produces only a slight peaking on such a plot.

Fig. 11 Invariant cross section for single particle (SPL) triggers obtained in this experiment compared to more precise data of other experiments.

Fig. 12 Scatterplot of P_T in the left and right arm for double arm (L + R) triggers at 400 GeV/c. The logarithmic intensity scale used for this plot suppresses the fact that P_T frequently balances. For comparison with hard quark scattering theories all events in the cross-hatched band are assumed to originate from fundamental quark scatters with the same P_T ($\sim$3.1 GeV/c in the figure).

Fig. 13 Solid Curve: True density of events in the cross-hatched band of figure 11 as a function of y', the distance from perfect P_T balance on the diagonal. Dashed Curve: Density of Monte Carlo events when each arm has an independent P_T spectrum satisfying previous single arm spectrometer experiments.

Fig. 14 Comparison of $d\sigma/dP_T$ for 200 and 400 GeV/c pp events giving double arm (L + R) triggers. The two sets of data would have the same slope if plotted as a function of x_T.

Fig. 15 Features of a jet model showing that average adjacent momenta are in the ratio 2:1 and that some fragments will always have a chance of being missed if internal transverse momentum in the jet is about 300 MeV/c.

Fig. 16 Distribution in P_T of the highest and second highest P_T segment of an event. These should be correlated with the P_T of individual particles in the jet. The ratio of P_T for the leading segments is $\sim$2:1.

Fig. 17 Comparison of measured multiplicity based on number of segment "hits" versus perdiction of jet model.

Fig. 18 Comparison of multiplicity versus P_T expected from soft pions and from data.

Fig. 19 Spectrum of measured jet masses for jets with $3.5 < P_T < 4.0$ GeV/c centered in a fiducial area of the right calorimeter.

Fig. 20 Monte Carlo model prediction for the average uncertainty in measurement of a jet direction because of missed fragments. No allowance is made for the possibility that a calorimeter "prefers" jets without missed fragments.

Fig. 21 Naive picture showing why parton structure functions tend to make both jets go forward in the πp center of mass system.

Fig. 22 Ratio of the number of pp to πp produced jets as a function of cms angles in double arm (L + R) triggers at 130 GeV/c. The p_T of a jet was between 2.5 and 2.75 GeV/c as defined in figure 11.

E395 JET EXPERIMENT

WISCONSIN

M. CORCORAN
A. ERWIN
E. HARVEY
R. LOVELESS
M. THOMPSON

PENNSYLVANIA

L. CORMELL
M. DRIS
B. ROBINSON
W. SELOVE
B. YOST
W. KONONENKO

LEHIGH

A. KANOFSKY
G. LAZO

FERMILAB

P. GOLLON

Figure 1

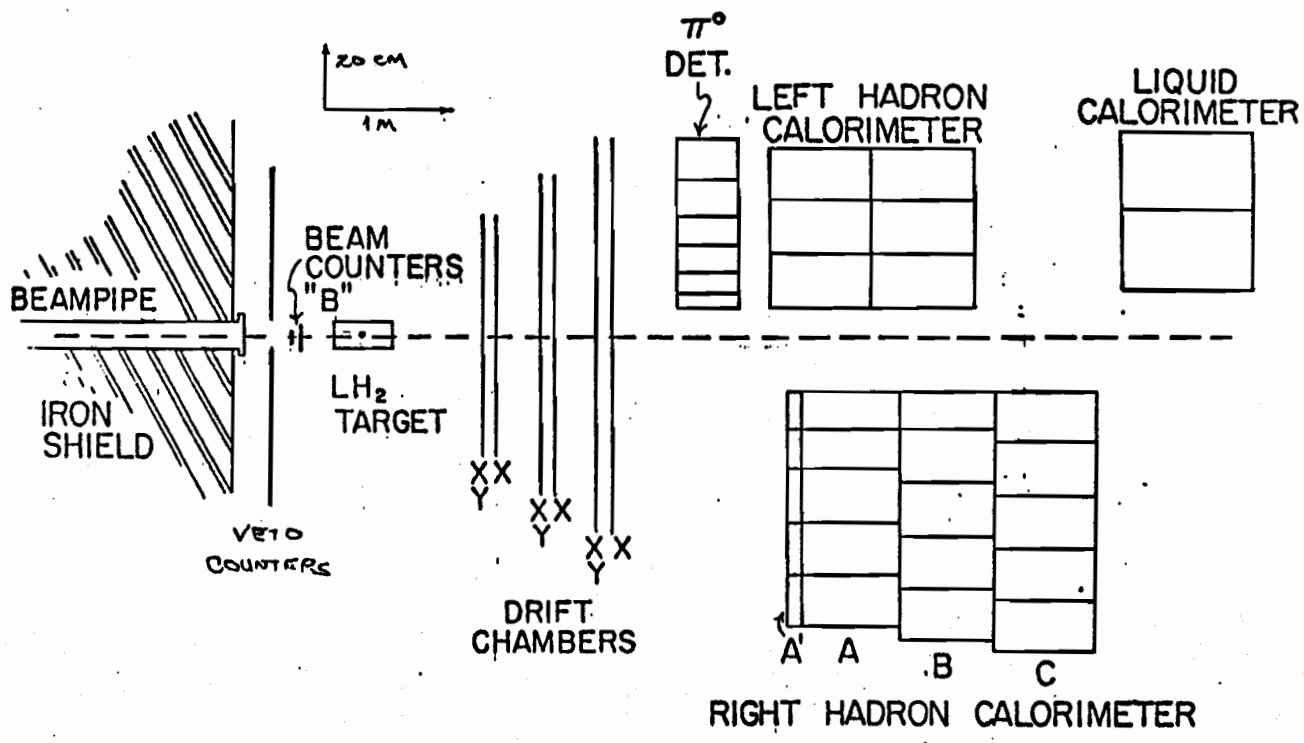
20 cm
1 m
BEAMPIPE
IRON SHIELD
VETO COUNTERS
BEAM COUNTERS "B"
LH2 TARGET
X X
Y
DRIFT CHAMBERS
π°
DET.
LEFT HADRON CALORIMETER
LIQUID CALORIMETER
A'
A
B
C
RIGHT HADRON CALORIMETER

Figure 2

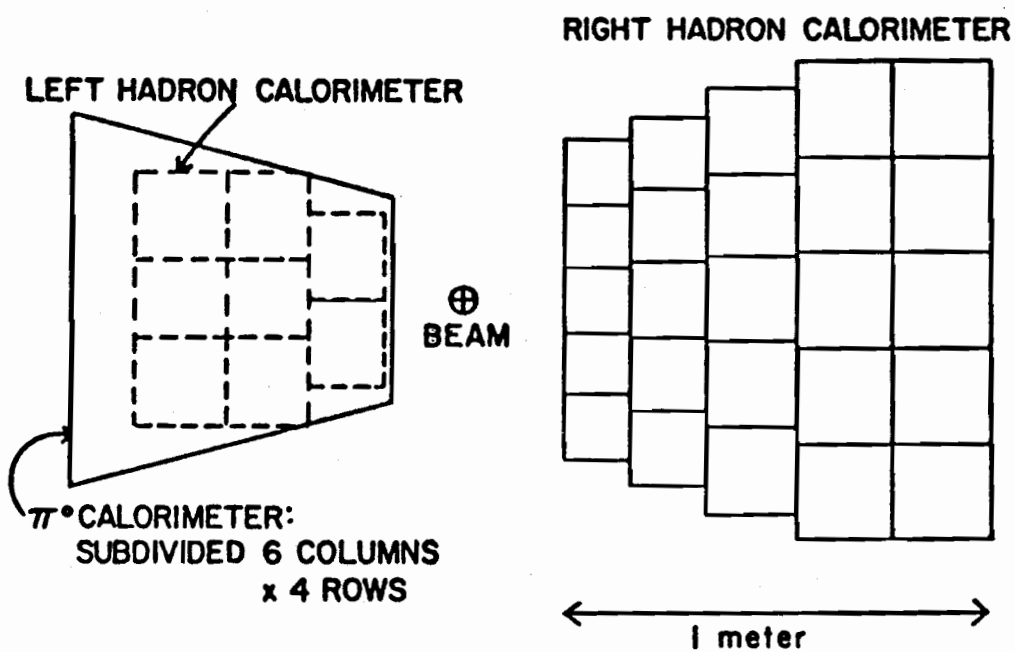
RIGHT HADRON CALORIMETER
LEFT HADRON CALORIMETER
⊕
BEAM
π° CALORIMETER:
SUBDIVIDED 6 COLUMNS
x 4 ROWS
1 meter

Figure 3

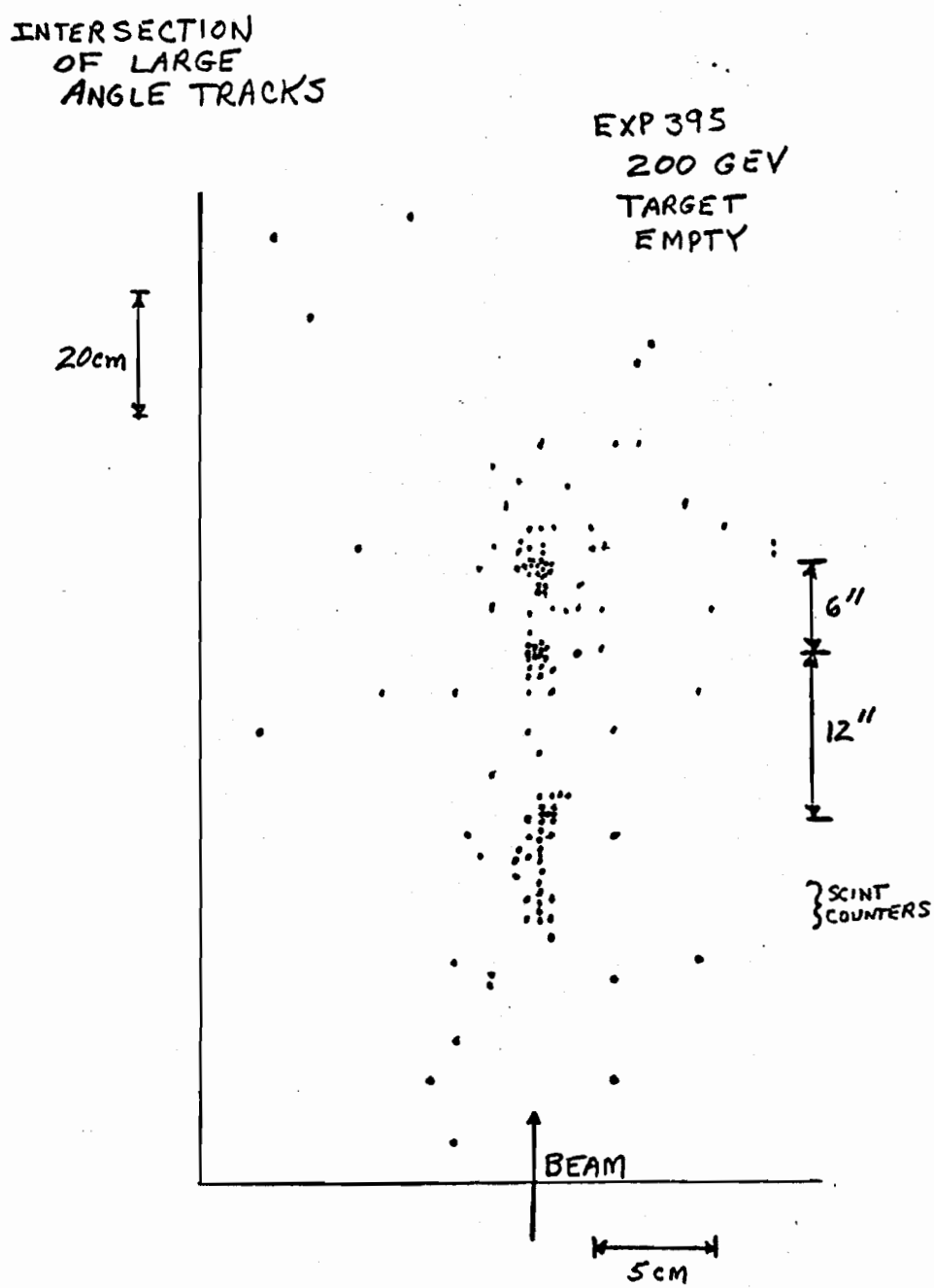
INTERSECTION
OF LARGE
ANGLE TRACKS
EXP 395
200 GEV
TARGET
EMPTY
20cm
6"
12"
SCINT
COUNTERS
BEAM
5cm

Figure 4

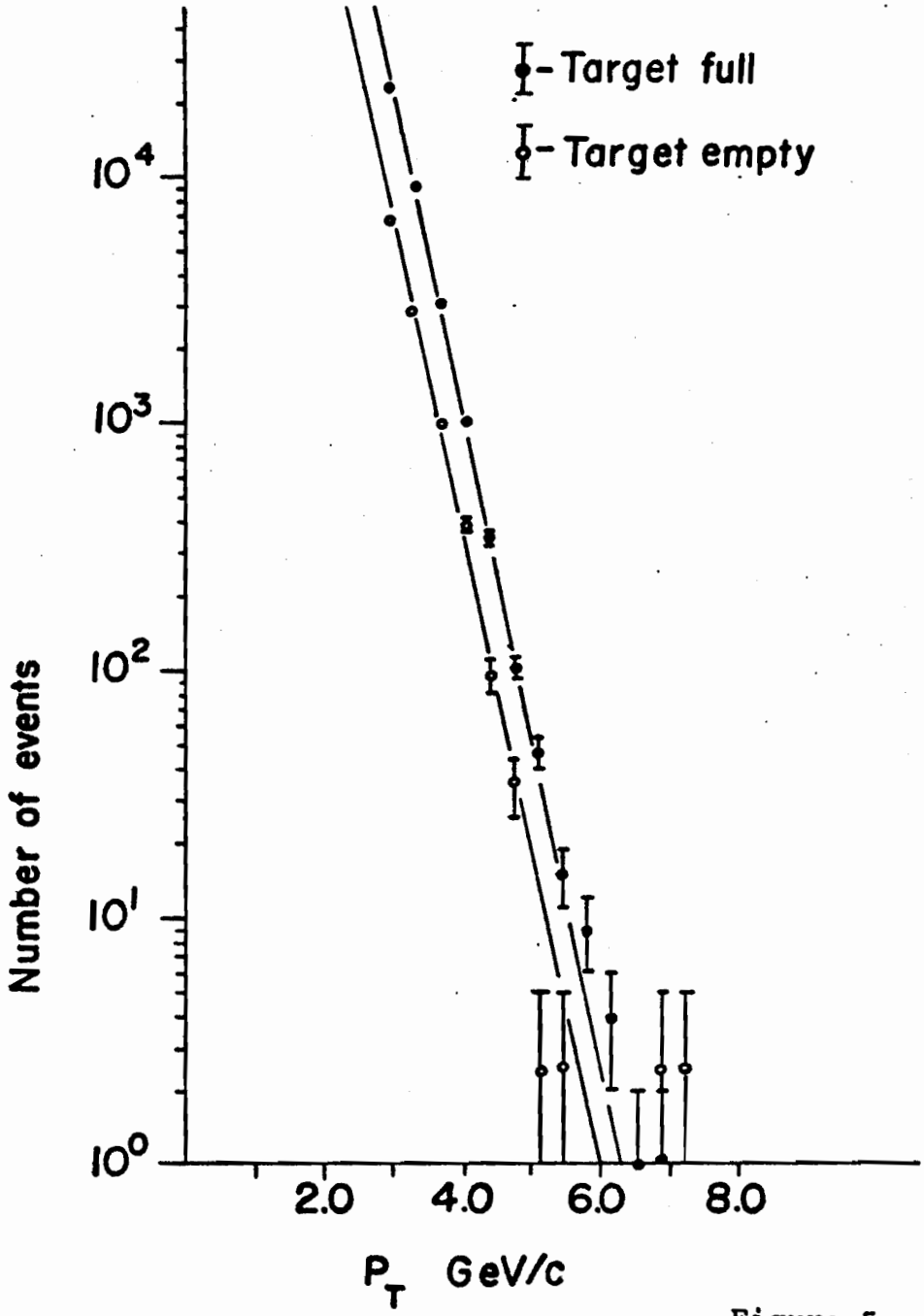
Target full
Target empty
Number of events
10^4
10^3
10^2
10^1
10^0
2.0
4.0
6.0
8.0
P_T GeV/c

Figure 5

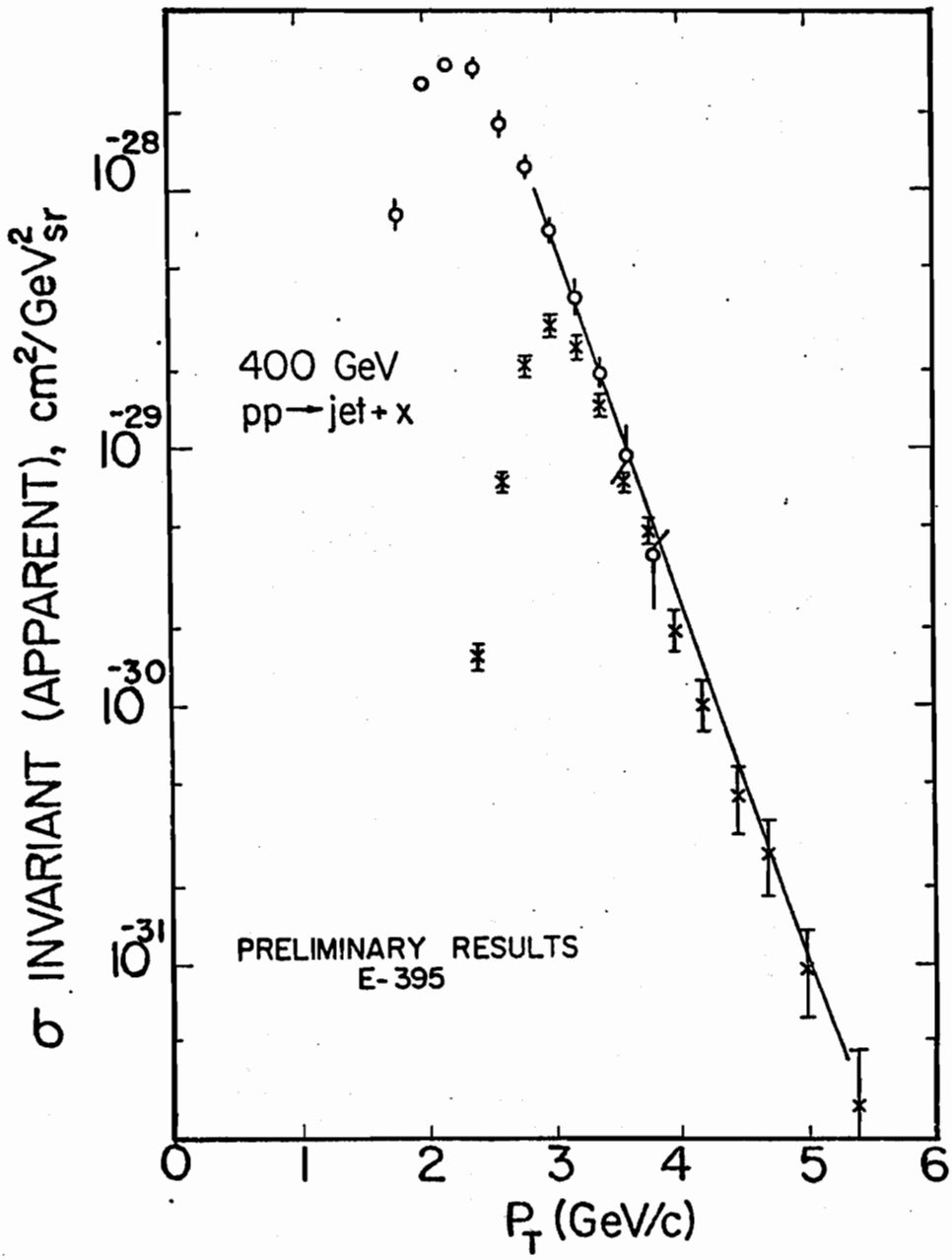
σ INVARIANT (APPARENT), cm²/GeV²sr
10⁻²⁸
10⁻²⁹
10⁻³⁰
10⁻³¹
400 GeV
pp→jet+x
PRELIMINARY RESULTS
E-395
0
1
2
3
4
5
6
P_T (GeV/c)

Figure 6

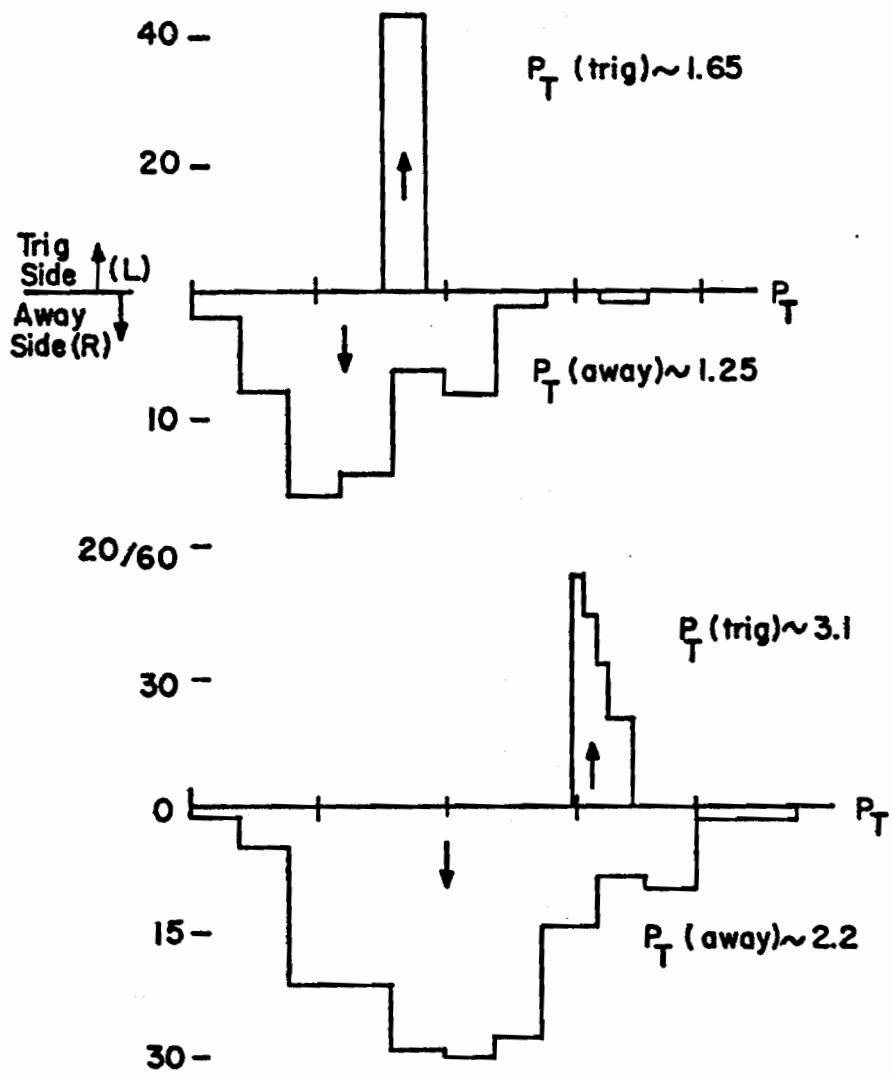

The Away-Side P_T Spectrum for Two P_T (trig) Bands

Figure 7

Preliminary Results - E 395

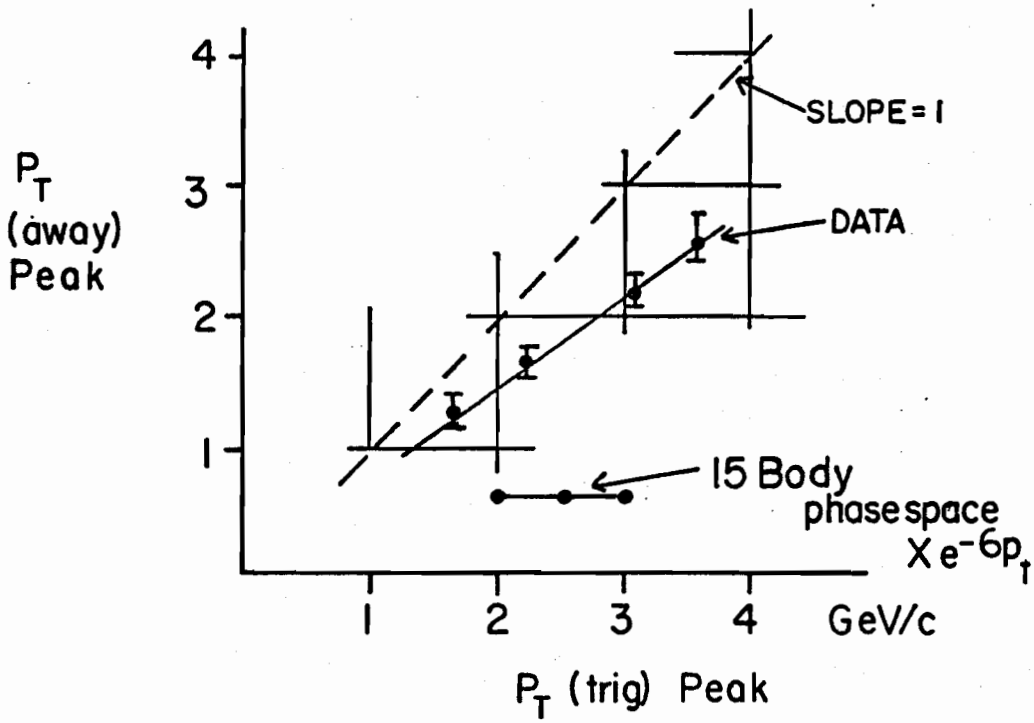

P_T (away) vs. P_T (trig)

Figure 8

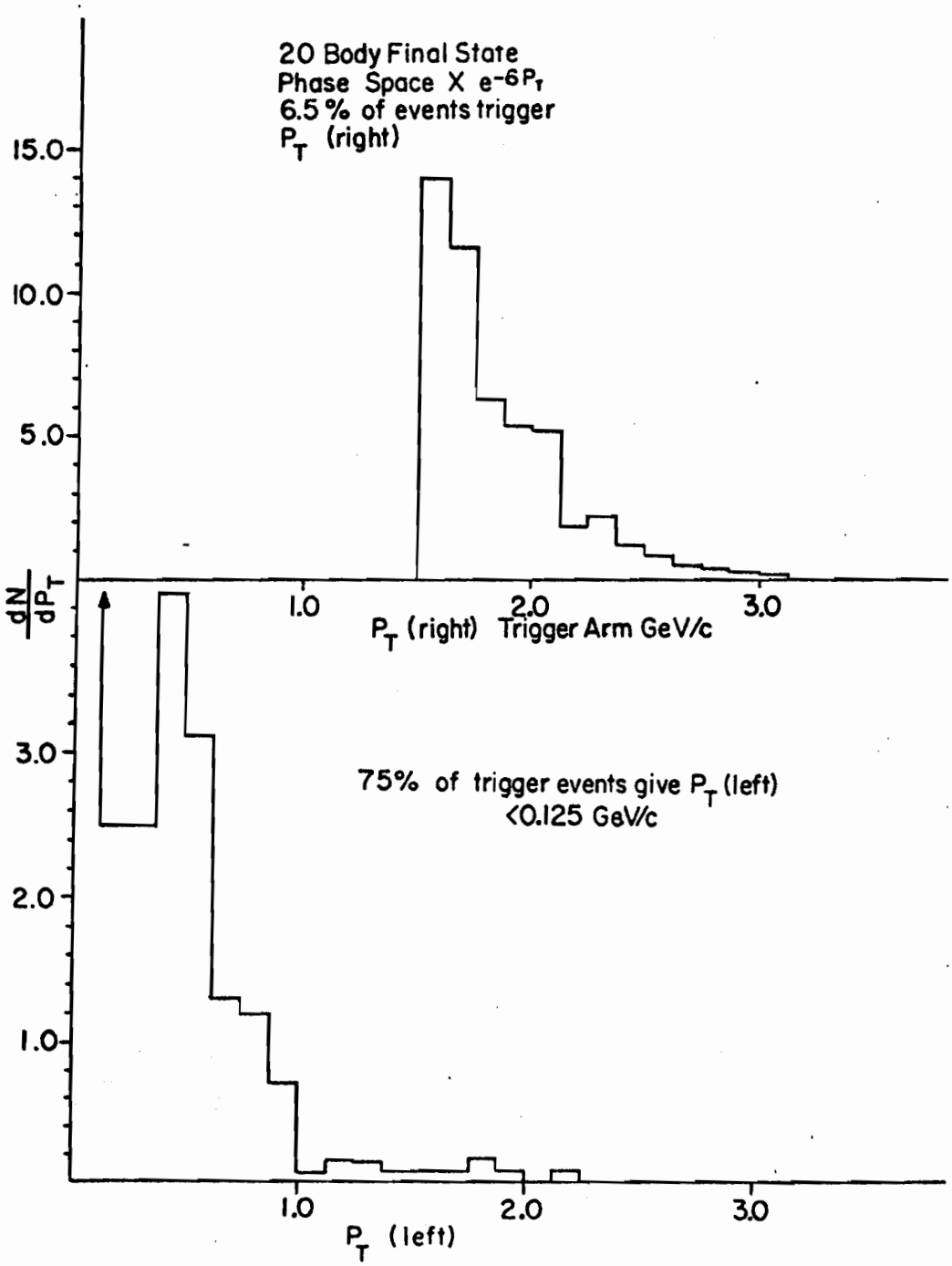
20 Body Final State
Phase Space X e^-6P_T
6.5 % of events trigger
P_T (right)
15.0
10.0
5.0
dN/dP_T
1.0
2.0
3.0
P_T (right) Trigger Arm GeV/c
3.0
2.0
1.0
75% of trigger events give P_T (left)
<0.125 GeV/c
1.0
2.0
3.0
P_T (left)

Figure 9

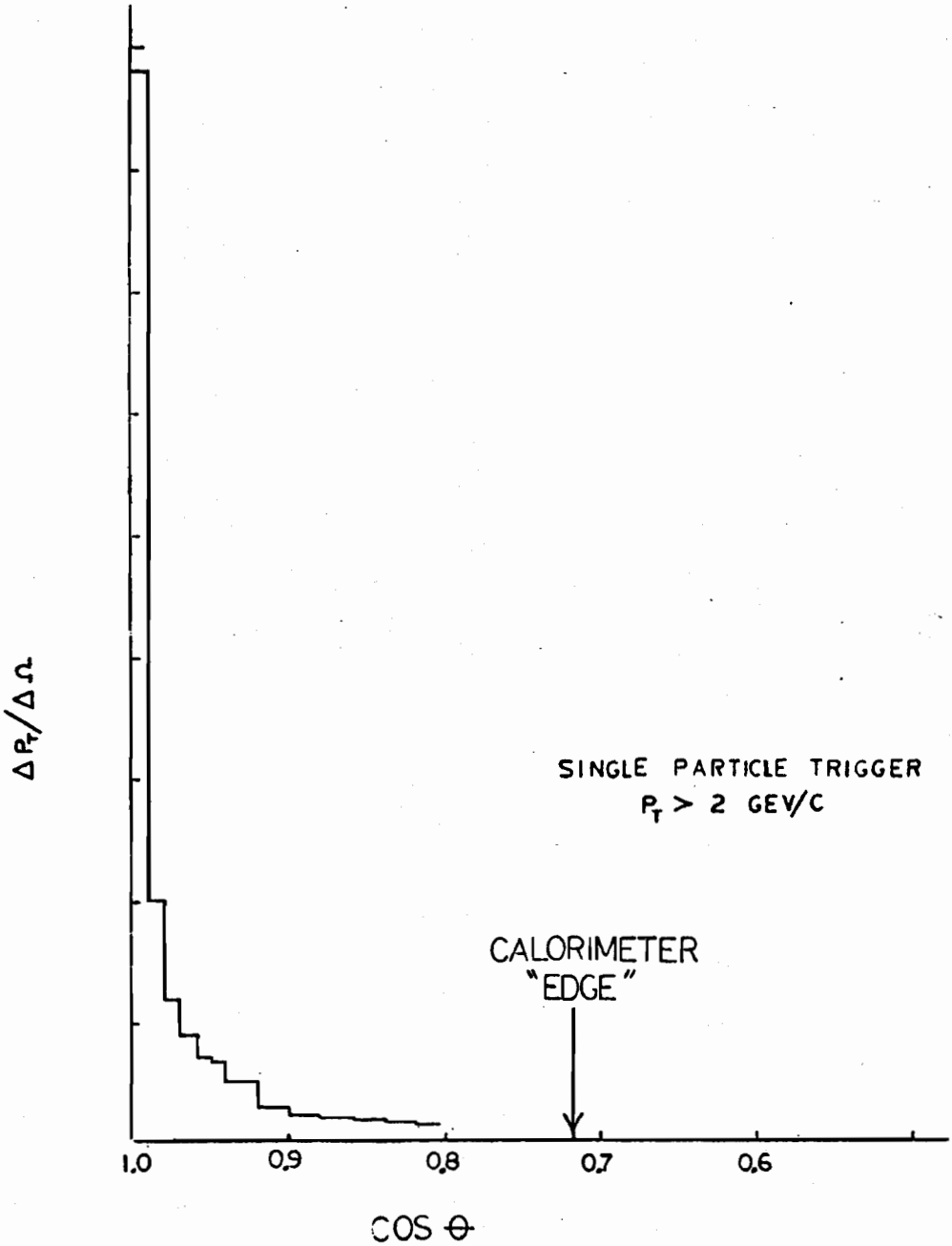
$\Delta P_T/\Delta\Omega$
SINGLE PARTICLE TRIGGER
$P_T > 2$ GEV/C
CALORIMETER
"EDGE"
1.0
0.9
0.8
0.7
0.6
COS θ

Figure 10

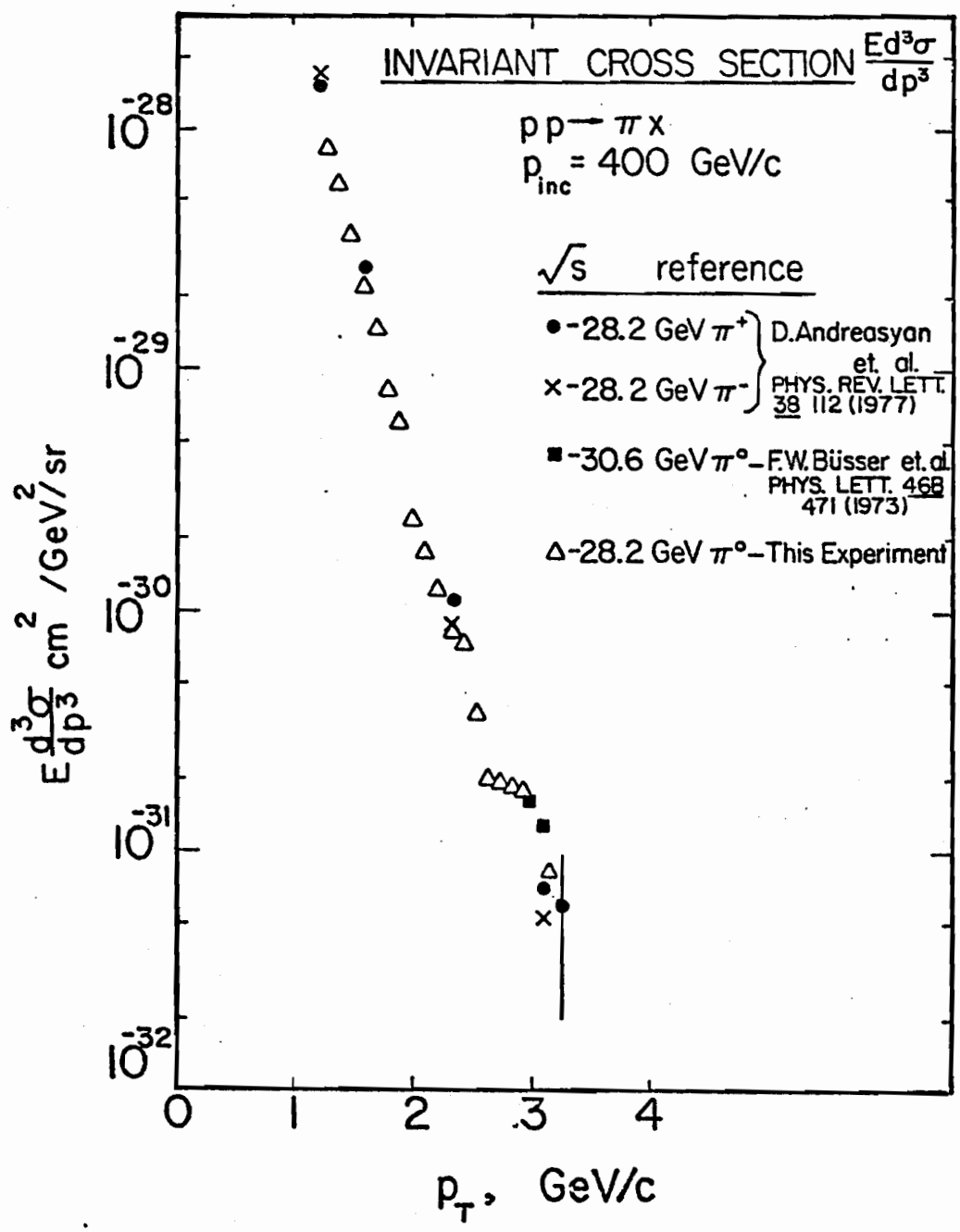
INVARIANT CROSS SECTION $E\frac{d^3\sigma}{dp^3}$
$pp \rightarrow \pi X$
p_{inc} = 400 GeV/c
$\sqrt{s}$ reference
●-28.2 GeV π^+
×-28.2 GeV π^-
D.Andreasyan et. al. PHYS. REV. LETT. 38 112 (1977)
■-30.6 GeV π^0-F.W.Büsser et.al PHYS. LETT. 46B 471 (1973)
Δ-28.2 GeV π^0-This Experiment
$E\frac{d^3\sigma}{dp^3}$ cm^2/GeV^2/sr
10^{-28}
10^{-29}
10^{-30}
10^{-31}
10^{-32}
0
1
2
3
4
p_T, GeV/c

Figure 11

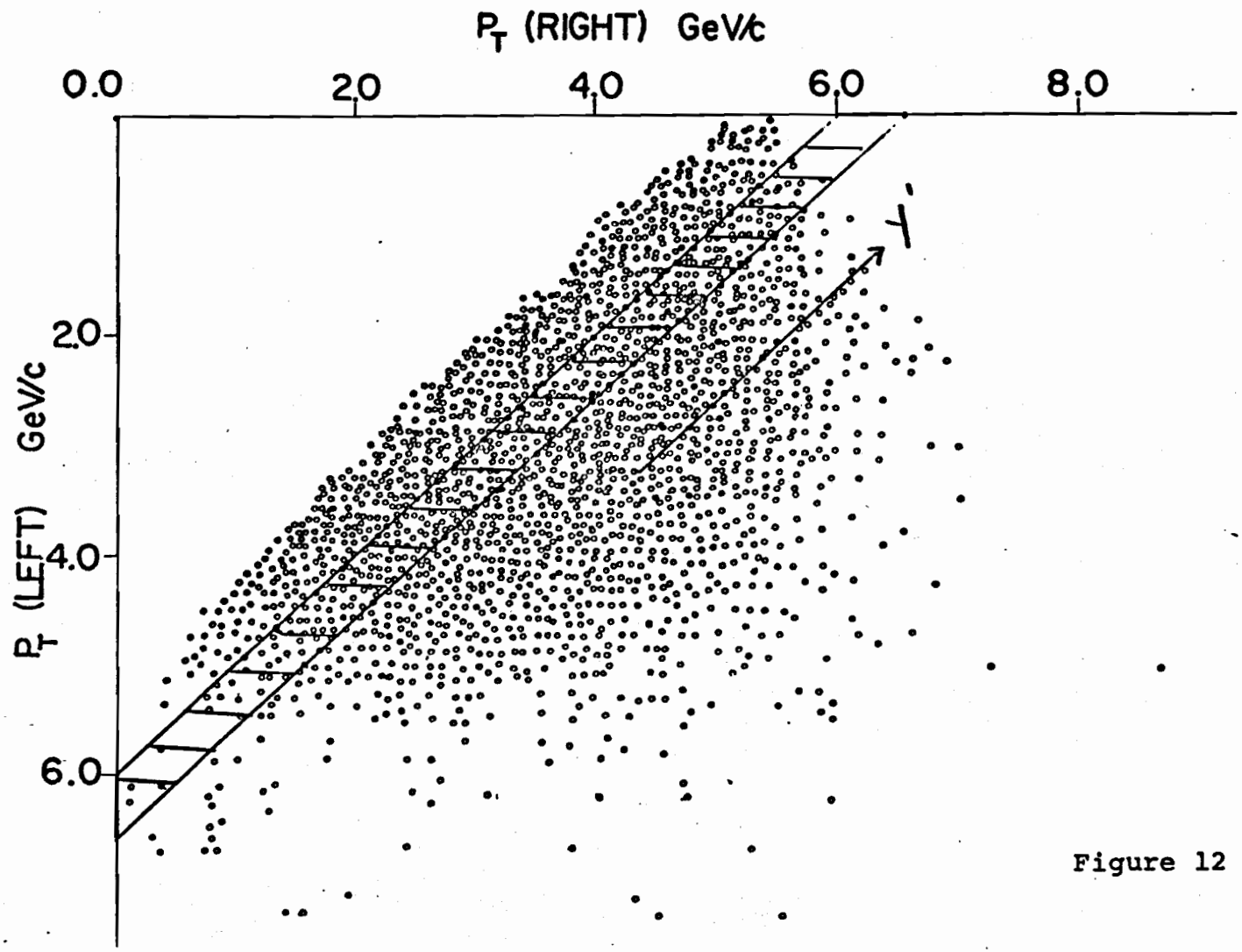

Figure 12

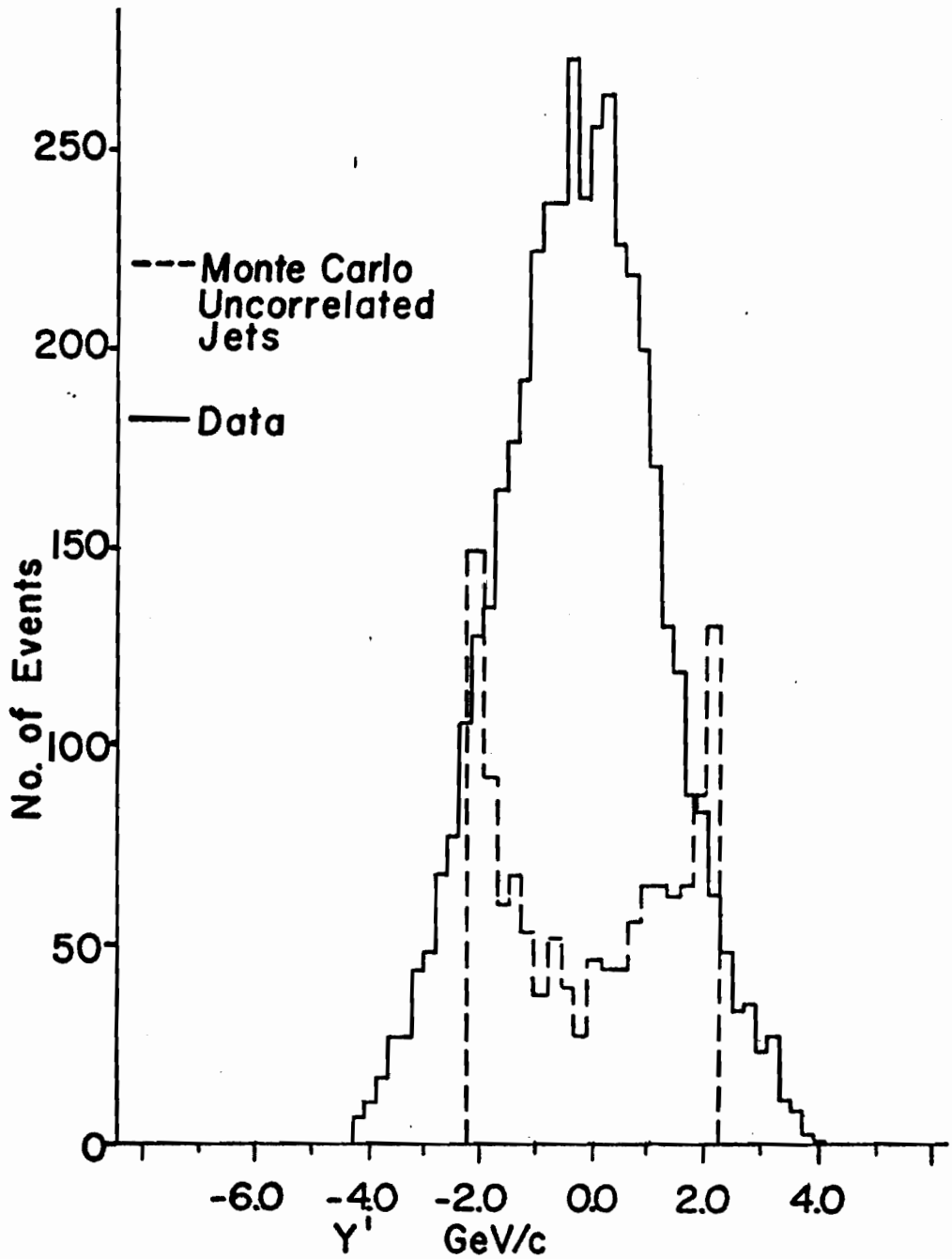
250
200
150
100
50
0
No. of Events
---Monte Carlo Uncorrelated Jets
—Data
-6.0
-4.0
-2.0
0.0
2.0
4.0
Y'
GeV/c

Figure 13

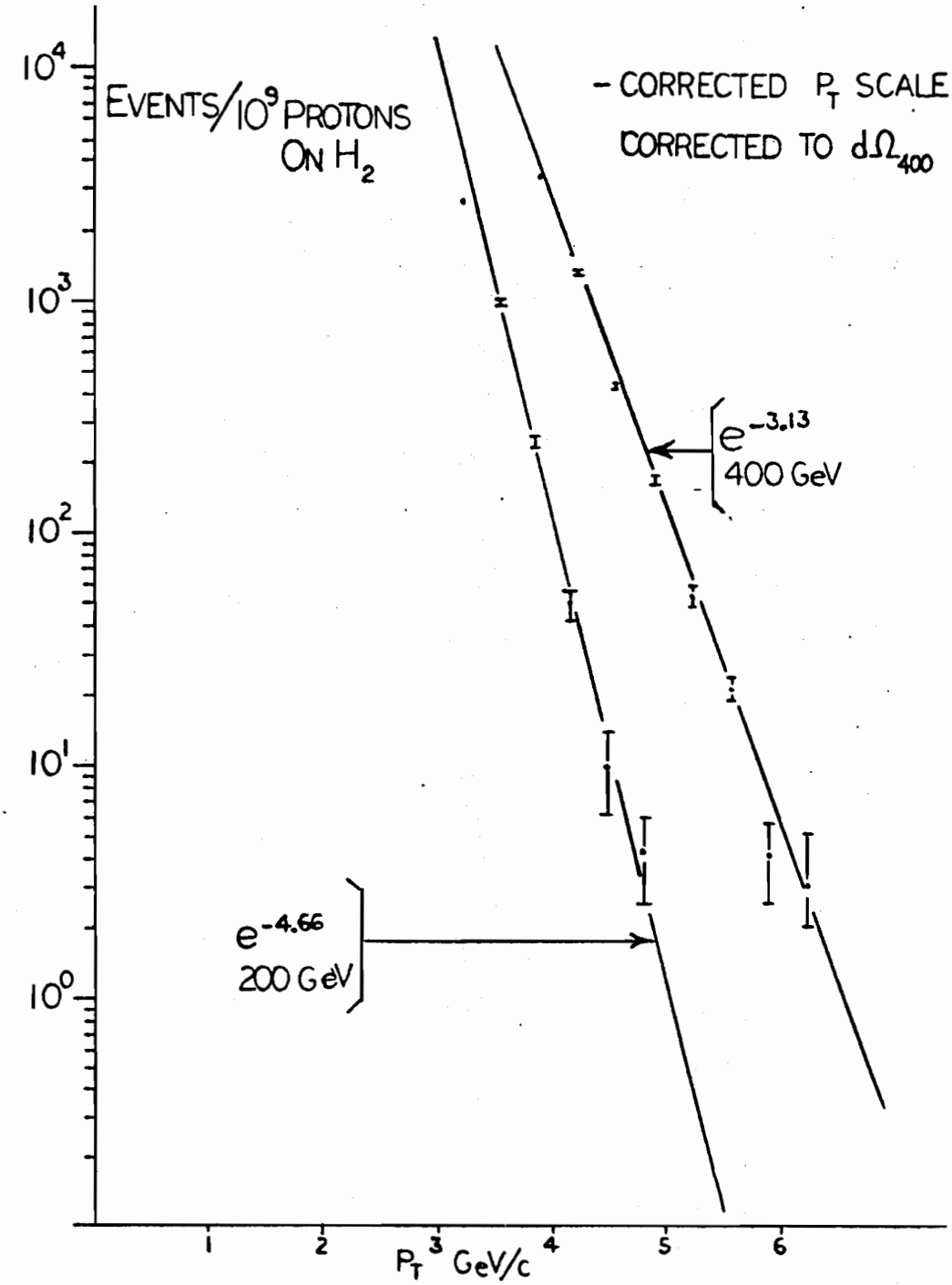
EVENTS/10^9 PROTONS ON H_2
- CORRECTED P_T SCALE
CORRECTED TO $d\Omega_{400}$
$e^{-3.13}$
400 GeV
$e^{-4.66}$
200 GeV
10^4
10^3
10^2
10^1
10^0
1
2
3
4
5
6
P_T GeV/c

Figure 14

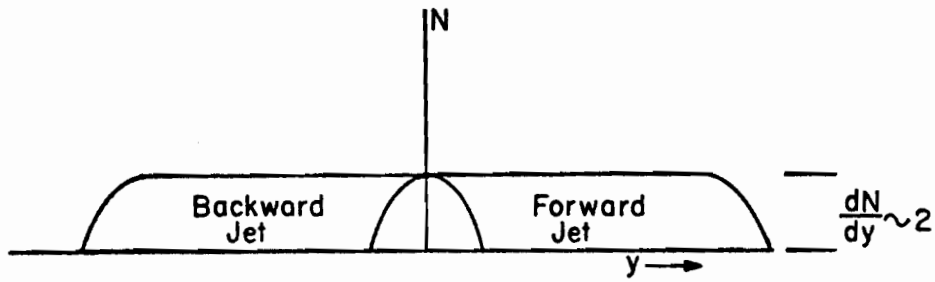

$$dN \sim 2(y^{n+1} - y^{n}) = 1$$

$$\frac{P_L^{n+1}}{P^{n}} \sim \frac{e^{y^{n+1}}}{e^{y^{n}}} \qquad y \gg 0$$

$$\sim e^{(y^{n+1} - y^{n})} \sim e^{1/2} \sim 1.65 \sim 5/3$$

$$\frac{P_L^{n}}{P_L^{n+1}} \sim .6 \longrightarrow .5$$

A Typical Jet

6 MeV = 3 + 1.5 + .75 + .325 + ……

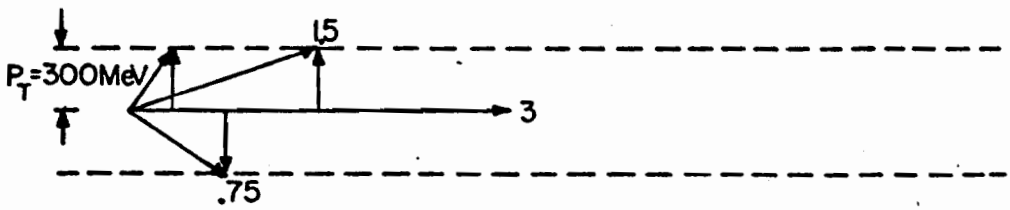

Figure 15

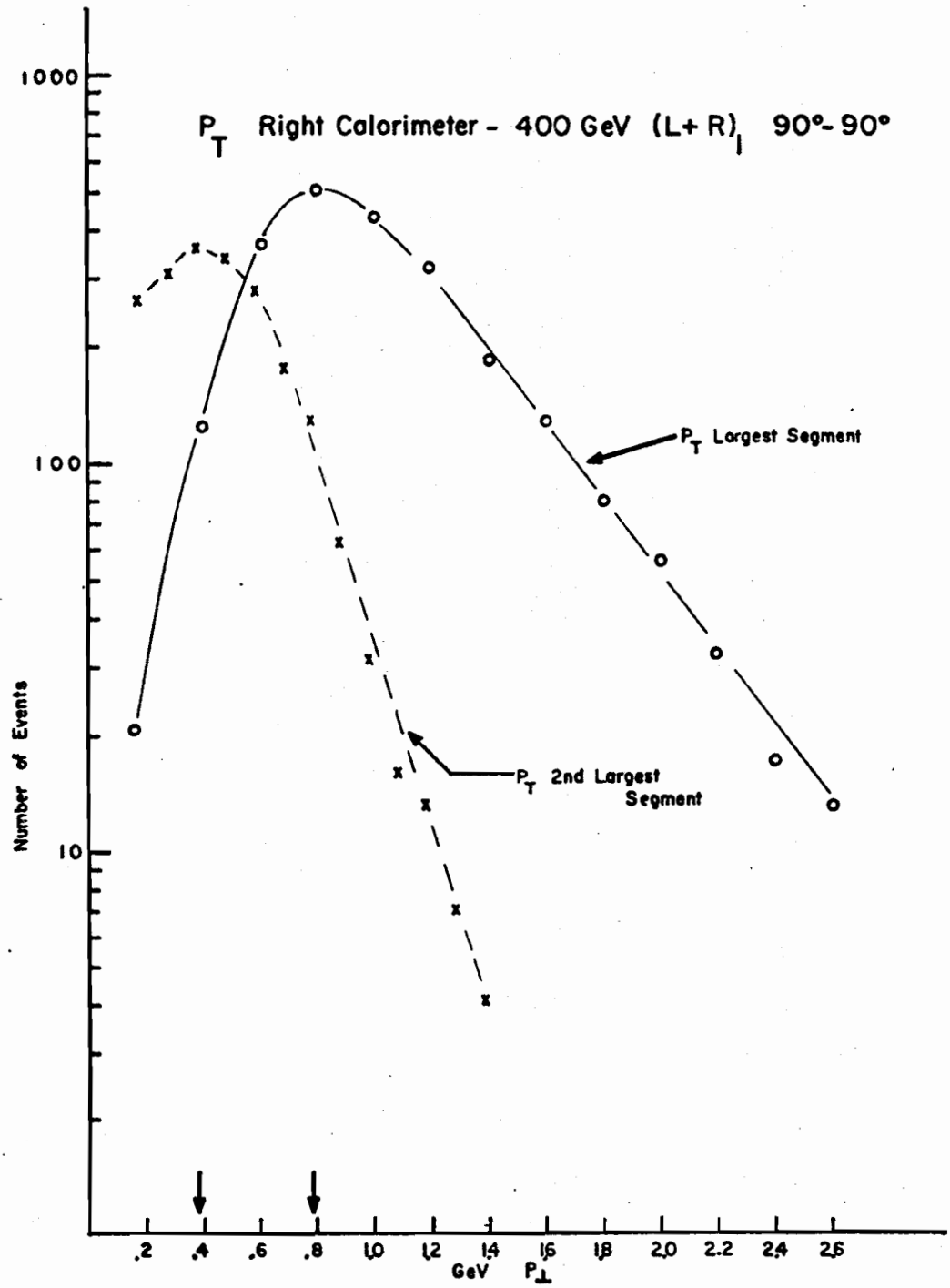
P_T Right Calorimeter - 400 GeV (L+ R)$_1$ 90°- 90°
1000
100
10
Number of Events
P_T Largest Segment
P_T 2nd Largest Segment
.2
.4
.6
.8
1.0
1.2
1.4
1.6
1.8
2.0
2.2
2.4
2.6
GeV $P_\perp$

Figure 16

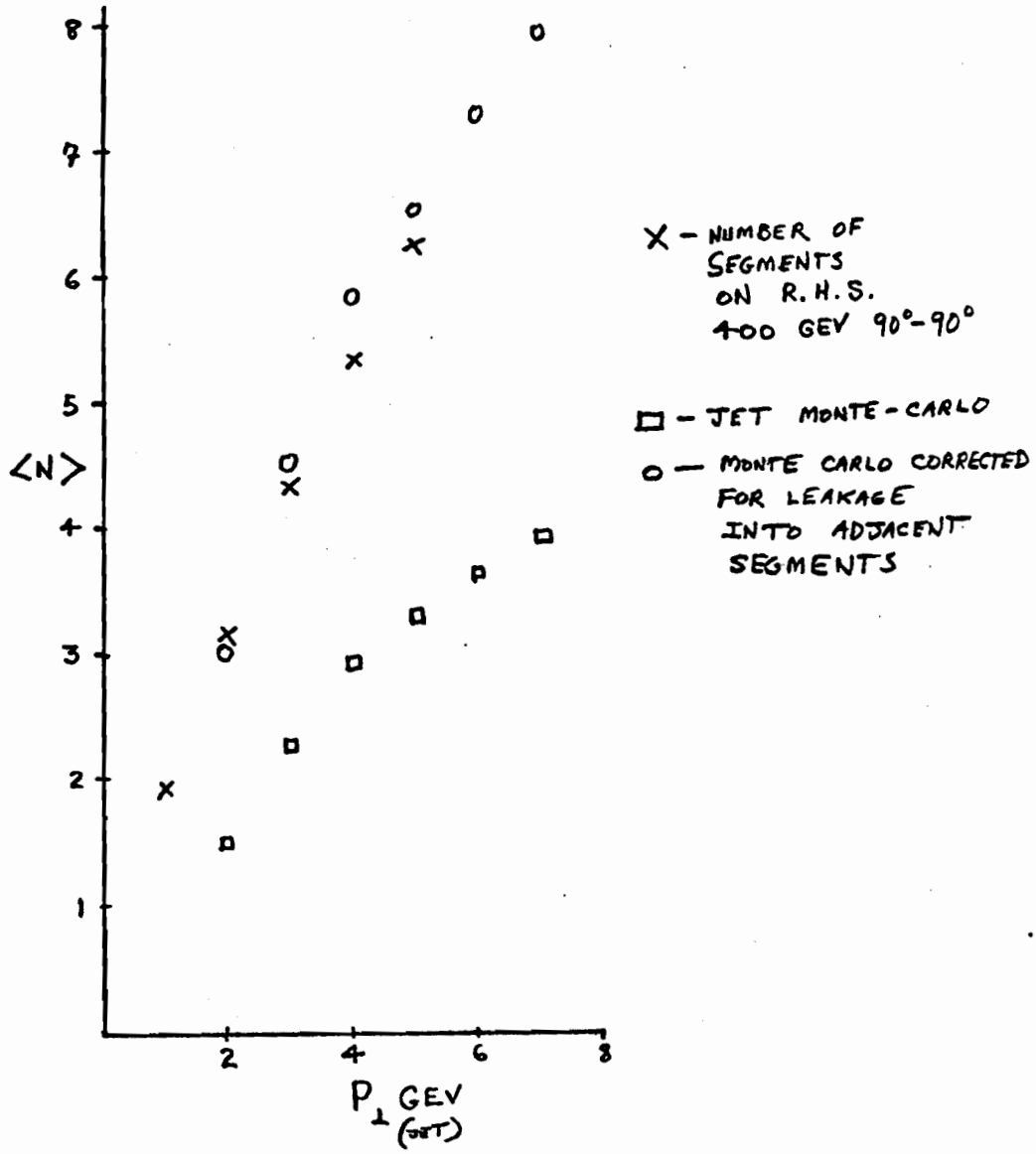
8
7
6
5
4
3
2
1
<N>
2
4
6
8
P⊥ GEV
(JET)
X - NUMBER OF SEGMENTS ON R.H.S. 400 GEV 90°-90°
□ - JET MONTE-CARLO
o — MONTE CARLO CORRECTED FOR LEAKAGE INTO ADJACENT SEGMENTS

Figure 17

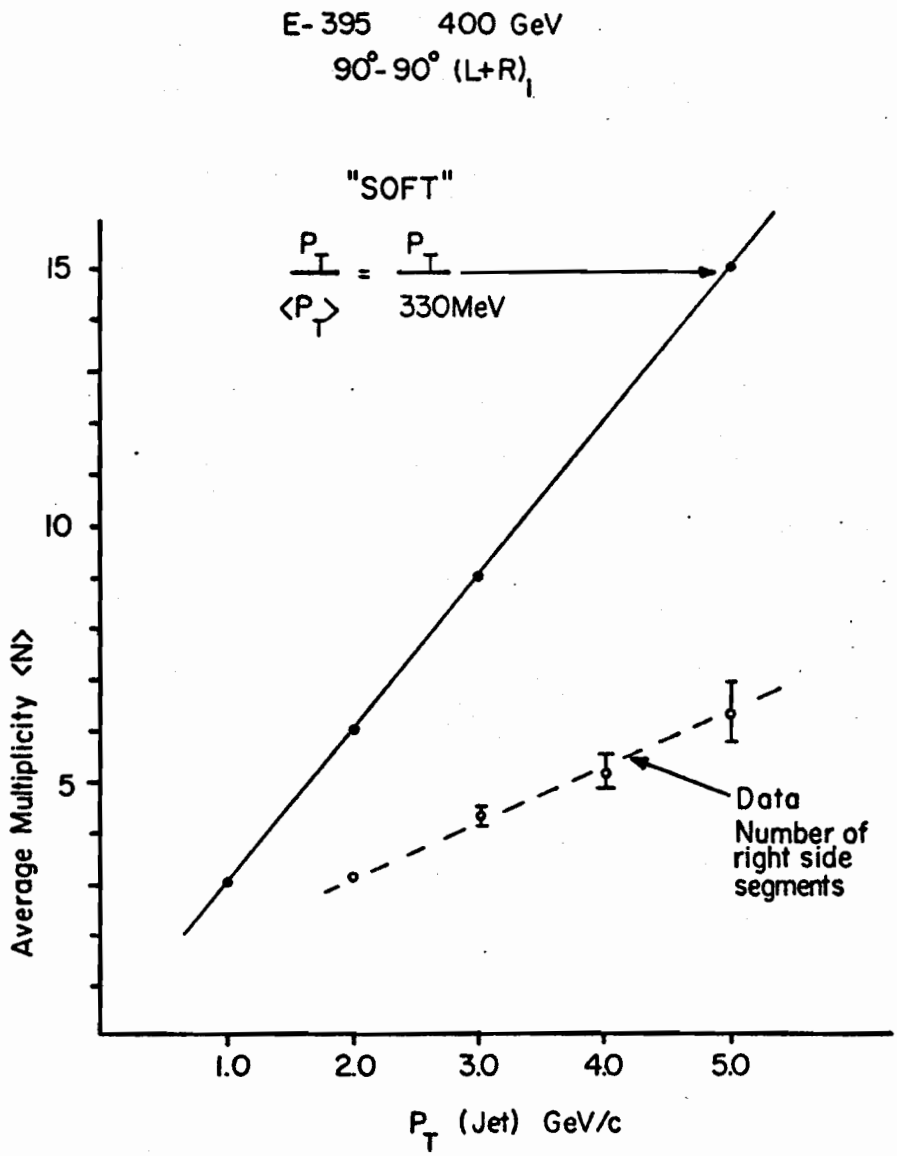
E-395 400 GeV
90°-90° (L+R)1
"SOFT"
PT / <PT> = PT / 330MeV
15
10
5
Average Multiplicity <N>
Data
Number of right side segments
1.0
2.0
3.0
4.0
5.0
PT (Jet) GeV/c

Figure 18

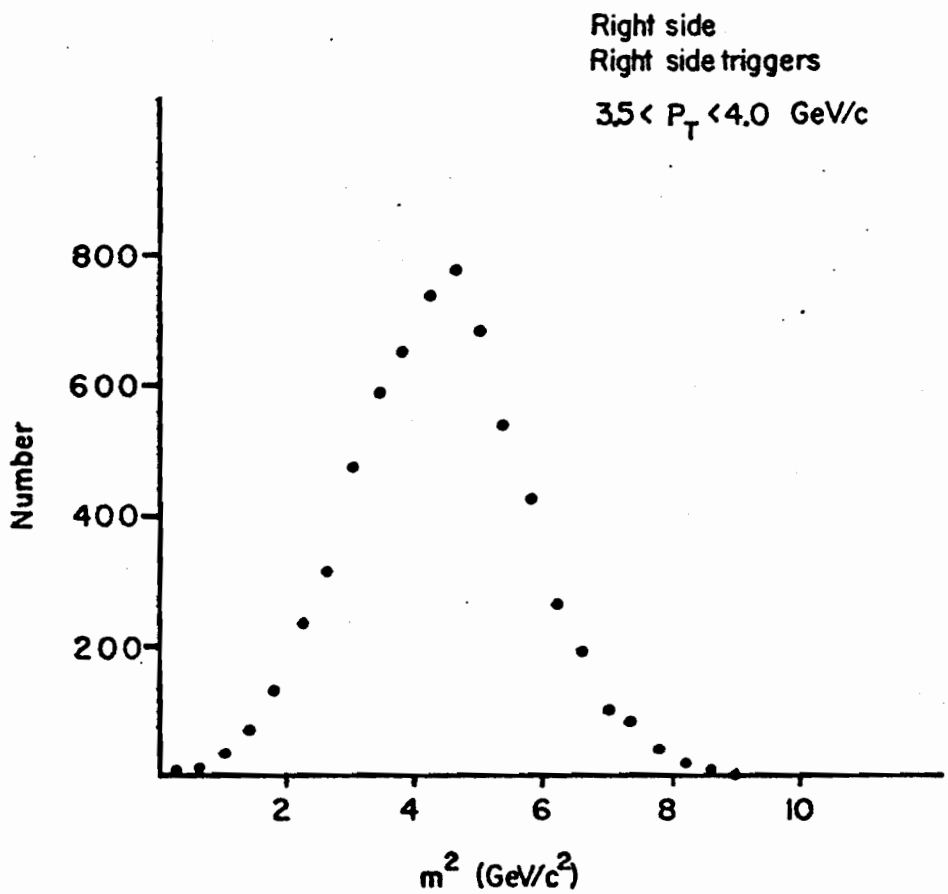
Right side
Right side triggers
3.5 < P_T < 4.0 GeV/c
800
600
400
200
Number
2
4
6
8
10
m^2 (GeV/c^2)

Figure 19

Monte Carlo Jets

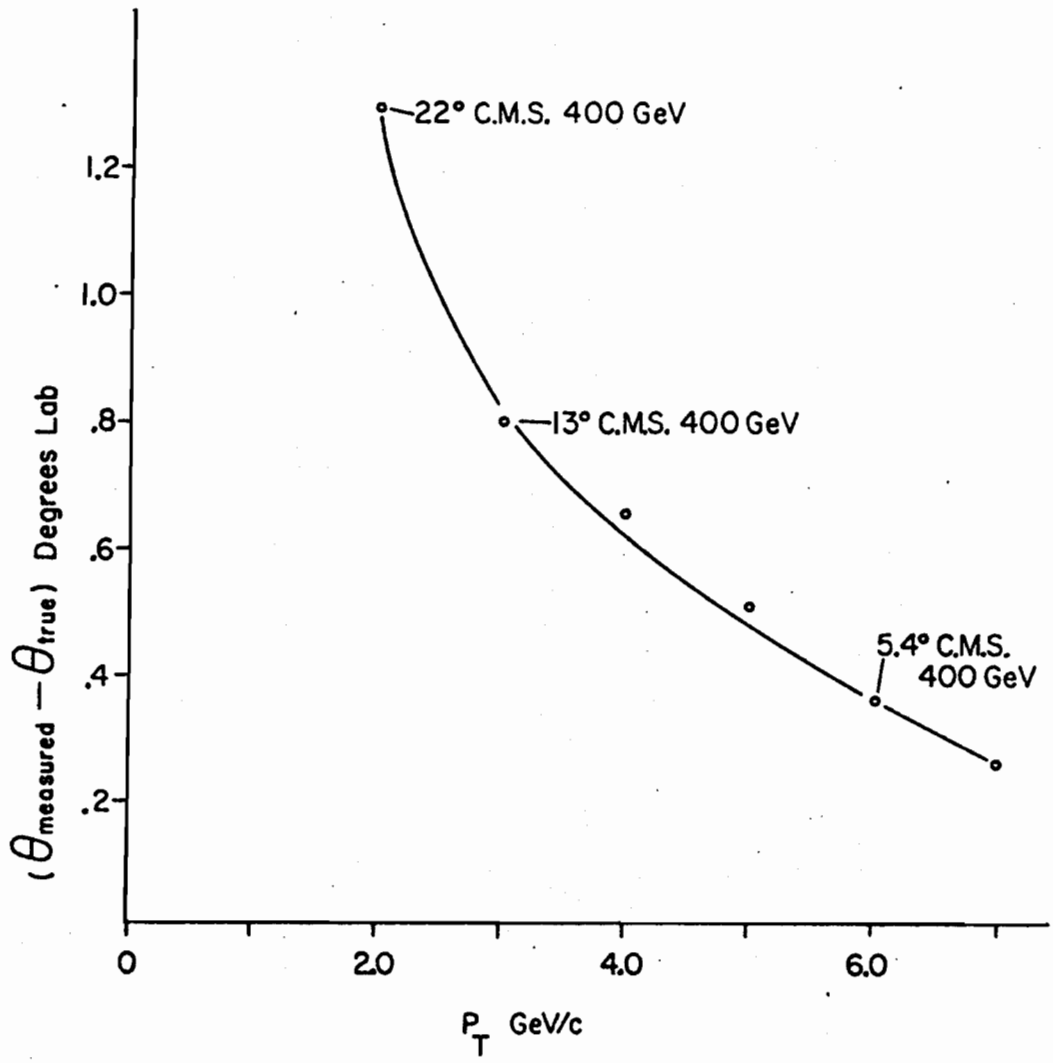

Figure 20

In Overall C.M.S.

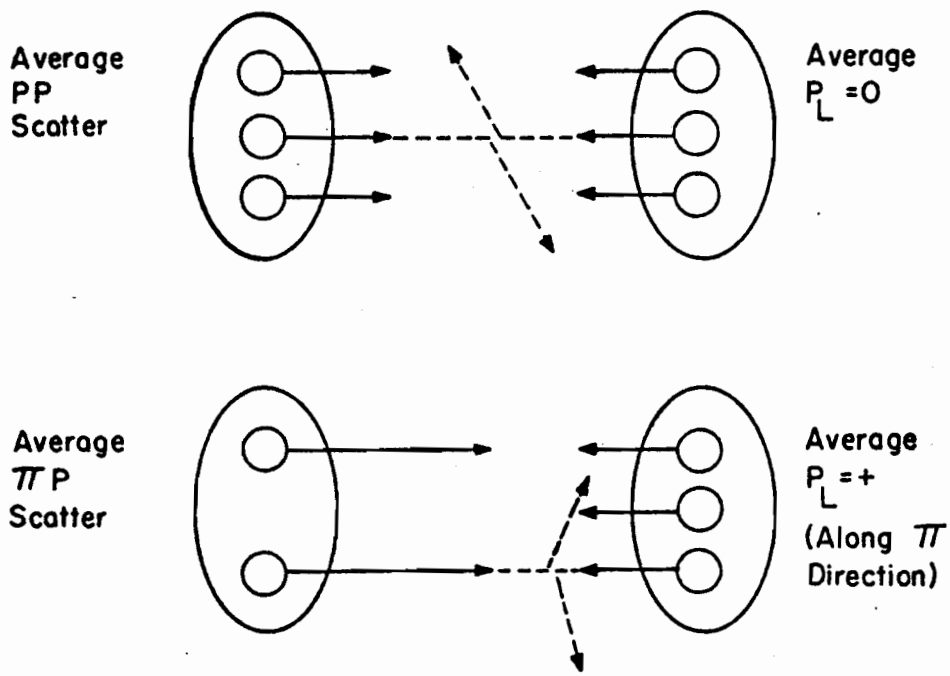

In the Overall C.M.S. one should find both jets in the forward hemisphere more frequently in πP collisions than in the PP collisions.

So plot

$$R(\theta_L^*, \theta_R^*) = \frac{\sigma(PP \rightarrow Jets)}{\sigma(\pi P \rightarrow Jets)}$$

Use P_T large enough to get angle definition in the C.M.S.

Figure 21

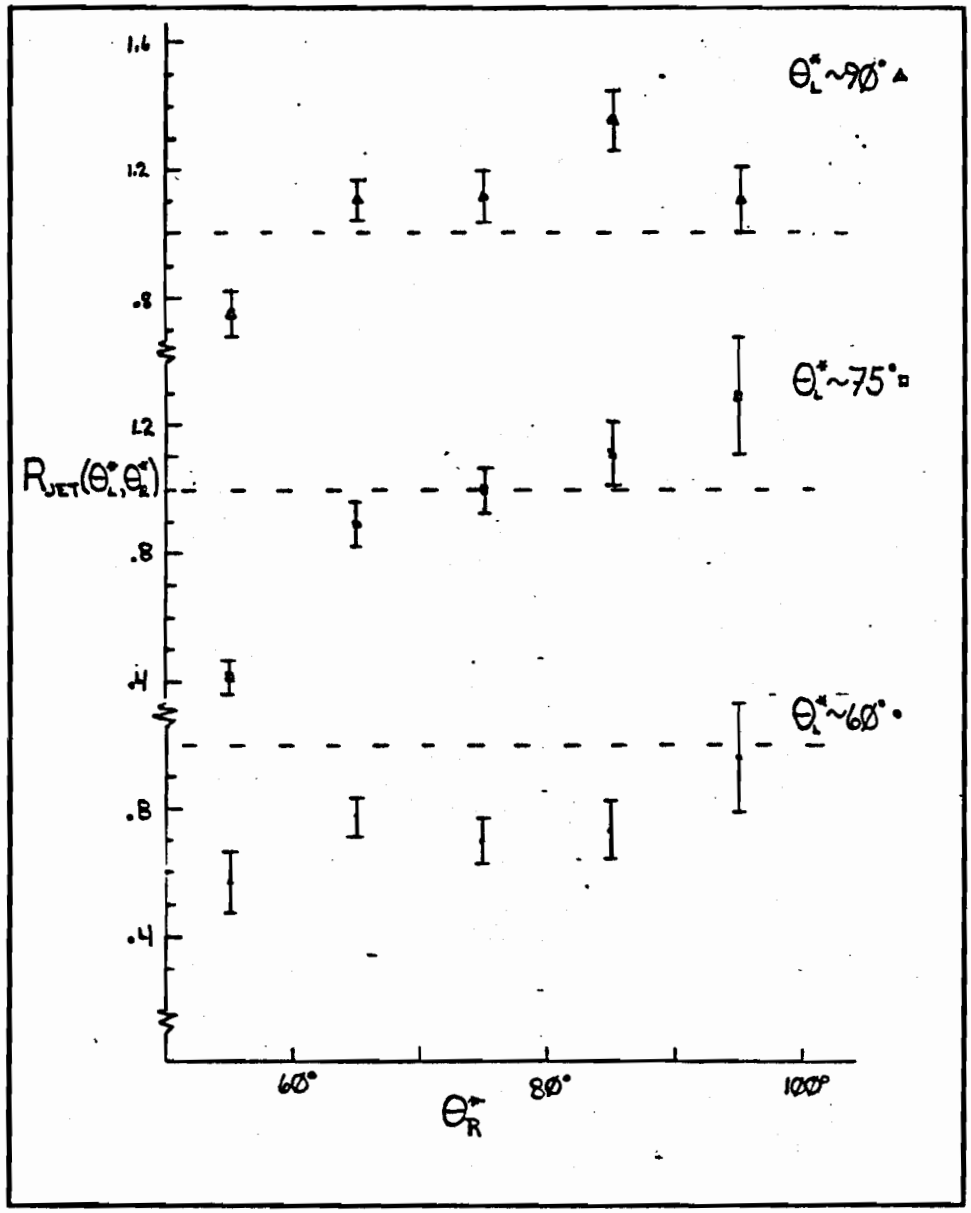
1.6
1.2
.8
1.2
.8
.4
.8
.4
$R_{JET}(\theta_L^*, \theta_R^*)$
$\theta_L^* \sim 90°$ ▲
$\theta_L^* \sim 75°$ ▫
$\theta_L^* \sim 60°$ •
60°
80°
100°
θ_R^*

Figure 22